Climatic Change (2020) 161:415–432
https://doi.org/10.1007/s10584-020-02654-0

New estimates of greenhouse gas emissions from biomass burning and peat fires using MODIS Collection 6 burned areas

Paolo Prosperi[1] · Mario Bloise[1] · Francesco N. Tubiello[2] · Giulia Conchedda[2] · Simone Rossi[3] · Luigi Boschetti[4] · Mirella Salvatore[1] · Martial Bernoux[1]

Received: 26 February 2019 / Accepted: 8 January 2020 / Published online: 7 February 2020

Abstract
The Paris Agreement calls on parties to undertake ambitious efforts to combat climate change by engaging in appropriate policies and measures as put forward through Nationally Determined Contributions (NDCs), to strengthen transparency when reporting their greenhouse gas (GHG) emissions and to increase their mitigation contributions to climate action from 2020. It also calls for regular and transparent monitoring and reporting of the GHG emissions and on the NDCs implementation efforts. Biomass fires significantly affect the GHG atmospheric balance, with fire emissions representing more than 5% of total emissions from agriculture, forestry, and other land use (AFOLU), according to recent estimates produced by the Food and Agriculture Organization (FAO). We update previously published Tier 1 estimates of GHG emissions in FAOSTAT—which had been used in the IPCC AR5 analysis—by using new burned area activity data from the Moderate Resolution Imaging Spectroradiometer (MODIS) known as MCD64A1, Collection 6. The previous FAOSTAT estimates had used as input the Global Fire Emission Database v.4 (GFED4) burned area product, based on older MODIS Collection 5.1 burned area product. In line with differences between the input data used, the new FAOSTAT estimates indicate roughly 30% higher fire emissions globally than previously published. Our analysis also confirms that the FAOSTAT Tier 1 approach produces fire emissions estimates that are comparable to those computed at Tier 3 by GFED, and thus represent a useful complementary tool in support of country GHG reporting.

Keywords Biomass burning · GHG emissions · MODIS burned area

✉ Paolo Prosperi
paolo.prosperi@fao.org

Extended author information available on the last page of the article

1 Introduction

Anthropogenic burning of biomass, including peatland, releases GHGs into the atmosphere (mainly CO_2, N_2O, and CH_4), leading to growing atmospheric concentrations and increased radiative forcing that induces climate change (Smith et al. 2014; Shi et al. 2015).

While it remains generally difficult to distinguish naturally ignited fires from anthropogenic ones (Levine 2010; EPA 2010), parties to the United Nations Convention on Climate Change (UNFCCC) have an obligation to periodically report their emissions from wildfires on managed land and human-induced fires. Reporting occurs through national inventories of GHGs that are part of the National Communications (NCs), Biennial Reports (BRs) or Biennial Update Reports (BURs), pursuant to the Convention (Articles 4 and 12) and relevant decisions of the Conference of the Parties (COP).

The recently enforced Paris Agreement and subsequent COP decisions further strengthened the request for parties for accurate reporting, introducing the new Biennial Transparency Reports and reiterating the five IPCC principles of transparency, accuracy, completeness, coherency, and comparability of GHG accounting (TACCC principles).

FAO aims at supporting countries, particularly the developing ones, in improving their national inventories as well as strengthening capacities to detect and accurately report burned areas and related GHG emissions. As part of this process, FAO disseminates yearly updates of national level emission/removal estimates for the Agriculture Forestry and Other Land Use (AFOLU) sector in FAOSTAT (see, e.g., http://www.fao.org/faostat/en/#data/GH and http://www.fao.org/faostat/en/#data/GI), following a Tier 1 methodology and approach 1 of land representation of the IPCC 2006 guidelines (Tubiello et al. 2013; Tubiello et al. 2014; Tubiello et al. 2019). Previous work (Rossi et al. 2016) demonstrated that the Tier 1 FAOSTAT GHG fire emissions estimates are comparable, globally and regionally, to Tier 3 estimates by GFED.

The most recent version (Collection 6—C6 in short) of the MODIS MCD64A1 Global Burned Area product (Giglio et al. 2018b; Boschetti et al. 2019) was employed in this study and to update the FAOSTAT emissions estimates. This MODIS product supersedes the previous version of the MODIS burned area product (MCD64A1 Collection 5.1, C5.1 in short). Both GEFD4 and previous FAOSTAT dataset were based on the MODIS C5.1 and both GFED and FAOSTAT fire emissions data underpinned relevant sections of the IPCC fifth Assessment Report (AR5) (Ciais et al. 2013), thus representing a critical source of information for regional and global level GHG estimates (Rossi et al. 2016). The present study aims at updating the FAOSTAT emissions as well as to compare the updated product to the most recent GFED emissions database (GFED4s) (van der Werf et al. 2017), helping countries to understand the differences between new and previous global greenhouse gas emission estimates products and therefore supporting efforts for transparent reporting under the Climate Convention.

While validation of the new C6 burned areas is discussed in Boschetti et al. (*in press*), a comparison between C6, C5.1, and GFED4s burned areas is also presented here as a potential factor affecting the related emission estimates levels.

2 Data and methods

2.1 Greenhouse gas emissions, burned areas, and land cover

As for the previous FAOSTAT version, this study calculates fire-related emissions applying a Tier 1 approach based on the 2006 IPCC Guidelines (IPCC 2006) but replacing GFED4 burned areas activity data with the new MCD64A1 C6 burned areas.

C6 burned area is being produced by the US National Aeronautics and Space Administration (NASA) using an improved version of the MCD64 burned area mapping algorithm (Giglio et al. 2009). The algorithm applies dynamic thresholds to composite MODIS Terra and Aqua imagery, generated from a burn-sensitive spectral band index derived from MODIS 1240 nm and 2130 nm Terra and Aqua surface reflectance, and a measure of temporal variability. Cumulative MODIS 1 km active fire detections are used to guide the selection of burned and unburned training samples and to guide the specification of prior burned and unburned probabilities (Giglio et al. 2018b). Compared to the previous C5.1 algorithm, the C6 algorithm features (Giglio et al. 2018a) are as follows: (*i*) improved detection of burned areas, especially of small burns (with a lower threshold of 100 ha ca.); (*ii*) reduced occurrence of unclassified grid cells and, in parallel, unique flagging of missing-data pixels versus water pixels; (*iii*) reduced temporal uncertainty of burn dates; (*iv*) expanded product coverage from 219 to 268 tiles; and (*v*) improved per-pixel quality assurance.

C6 burned area is distributed as a monthly, level-3 gridded 500-m product containing per-pixel burning date and quality information.

Temporal and areal uncertainty of the C6 product are illustrated in Giglio et al. (2018b) and an intercomparison of four global burned area products, including C6, is discussed in Humber et al. (2019), who also give indications on which products, among those analyzed, most reasonably capture the burning regime.

In our study, consistently with the previous version of FAOSTAT, the land cover information data was retrieved from the MODIS Global Land Cover Product (MCD12Q1 Collection 5.1, Friedl et al. 2010) for the available years (2001–2013). For years beyond 2013, it was assumed that no land cover change occurred compared to 2013 due to unavailability of more recent MCD12Q1 data.[1] The MCD12Q1 product is generated using 5 different land cover classification schemes; in the present study, the University of Maryland (UMD) classification scheme was considered.

Processing of the full time series of original C6 monthly tiles for the extraction of the burned areas by land cover consisted of the following operations: (*i*) preliminary filtering to extract only valid burn dates: any value (calendar day) between 1 and 366 was considered valid; (*ii*) transformation of valid burn dates into per-pixel fire count: any day between 1 and 366 was counted as one fire occurred; (*iii*) transformation of fire counts into burned area surface: this was obtained by multiplying the non-zero fire counts by the pixel surface area, equal to a constant 21.46 ha (pixel X size × Y size) across the globe due to the MCD products' sinusoidal projection (equal-area); (*iv*) partitioning of the monthly burned area tiles by land cover.

[1] The MCD12Q1 was decommissioned immediately after this research was completed and replaced with C6—https://lpdaac.usgs.gov/about/decommissioning_modis_version_51_land_cover_type_data_products_january_7_2019

Following the previously published FAOSTAT methodology (Rossi et al. 2016), C6 monthly burned areas tiles were converted into yearly burned areas tiles (summing up the twelve monthly files), and then mosaicked globally by UMD land cover class.

More precisely, the five UMD land cover classes representing forests (class 1: evergreen needleleaf; class 2: evergreen broadleaf; class 3: deciduous needleleaf; class 4: deciduous broadleaf; class 5: mixed forests) were aggregated to form the three forest-based classes boreal, temperate, and tropical to allow for calculation of the emissions and then further aggregated as "humid tropical forest" and "other forest" for comparison with GFED4s (Rossi et al. 2016).

As for the former FAOSTAT version, burned areas occurring in the cropland land cover class were excluded from the analysis due to the high uncertainty in mapping agricultural burning compared to other land cover classes (Giglio et al. 2018a, b; Zhu et al. 2017; Hall et al. 2016; Zhu et al. 2017).

For peatlands, the FAOSTAT methodology was applied, deriving the map of histosols from the Harmonized World Soil Database (HWSD) (FAO/IIASA/ISRIC/ISSCAS/JRC 2012) as a robust proxy for peatlands (Egglestone et al. 2006) and independently from the MCD12Q1 land cover product. Unlike earlier version, in this study, pixel resampling and reprojection of the map of histosols followed the MCD64A1 specifications. The map of burnt peatlands was thus derived overlaying the map of histosols with the C6 burned areas. The overlay is independent from land cover information, i.e., estimates of fires in peatlands are a combination of fires in all possible types of land cover on organic soils.

The newly generated yearly global mosaics of burned areas by land cover class (plus peatland) were then used as a basis for our analyses. The burned areas were compared with those from C5.1 (extracted from GFED4 burned areas at 0.25° resolution used in the previous FAOSTAT dataset), by land cover class and peatland, globally, and by GFED region.

A further comparison was added with GFED4s burned areas (partitioned using the same land cover datasets and classes as FAOSTAT) as this may offer a good insight into the differences in related emissions with those in previous and current version of FAOSTAT. However, it has to be noted that, opposite to GFED4s emissions, GFED4s burned areas are only distributed as annual global values; therefore, our partitioning did not necessarily produce the same activity data used to generate GFED4s emissions, particularly in the case of peatland.

2.2 Fuel biomass consumption values and emission factors

This study calculates all emission estimates from C6 burned areas using the fuel biomass consumption values and emission factors derived from the IPCC 2006, following the same methods presented in Rossi et al. (2016). As in Rossi et al. (2016), the aggregated land cover classes described above in Section 2.2 were combined with the Joint Research Centre (JRC) climate map to locate spatially fuel biomass values and emission factors by vegetation type and climate zones; in the present study, the climate map was resampled at 500 m ground resolution rather than at the 0.25° resolution previously used.

The fuel biomass consumption values and emission factors are reported in Table 1. As a reference, Table 1 reports also the field-derived consumption values summarized from the available literature by van Leeuwen (2014).

Table 1 Biomass consumption and emission factors from the 2006 IPCC guidelines used in the present study, as reported by Rossi et al. (2016), and field-derived biomass consumption compiled from literature (van Leeuwen et al. 2014, Table 3). Standard deviation (SD) is reported in parenthesis

Fire emission source	IPCC biomass consumption	Field-derived biomass consumption	IPCC emission factors		
	($t\ ha^{-1}$)	($t\ ha^{-1}$)	($g\ kg^{-1}$)		
			N_2O	CH_4	CO_2
Savanna (tropical)	7	4.6 (2.2)	0.21	2.3	1613
Savanna (non-tropical)	4.1		0.21	2.3	1613
Woody savanna (tropical)	6	5.1 (2.2)	0.21	2.3	1613
Woody savanna (non-tropical)	3.3		0.21	2.3	1613
Grassland (tropical)	5.2	4.3 (2.2)	0.21	2.3	1613
Grassland (non-tropical)	4.1		0.21	2.3	1613
Open shrublands	14.3	32 (19)	0.21	2.3	1613
Closed shrublands	26.7		0.21	2.3	1613
Forest (boreal)	41	39 (19)	0.26	4.7	1569
Forest (temperate)	50.4	93 (79)	0.26	4.7	1569
Forest (tropical)	54.1	126 (77)	0.2	6.8	1580
Peatlands (tropical)	353	314 (196)	0.2	20.8	1703
Peatlands (boreal and temperate)	66	42 (–)			

2.3 Emissions

New estimates of GHG emissions from burning of biomass were computed for each of the source classes using the FAOSTAT methodology and parameters ("FAOSTAT emissions") along with the new yearly C6 burned areas (Rossi et al. 2016) and were then re-aggregated to allow for comparison with GFED4s emissions data (Table 2).

More in detail, using the FAO Global Ecological Zones (FAO-GEZ) map, the new emissions from the forest land cover classes (boreal, temperate, tropical) were aggregated into "humid tropical forests" (masking against the FAO-GEZ classes 11, tropical rainforest; and 12, tropical moist forest) and "other forests" (all other FAO-GEZ classes). Following the GFED approach, burning of humid tropical forests was used as a proxy for the GFED4s "deforestation and forest degradation" class (Rossi et al. 2016) while fire emissions from the remaining forests ("Other forest") were compared against the GFED4s "boreal and temperate class."

Table 2 Mapping of GFED4s classes of emissions to new FAOSTAT emissions

GFED4s emission source classes	Process followed to derive the corresponding new FAOSTAT emissions	
	Step 1	Step 2
Tropical deforestation and degradation	Sum of emissions from all forest classes (boreal, temperate, tropical)	Sum of emissions from step 1 clipped on the humid tropical class (tropical rainforest and tropical moist forest classes) from the GEZ-FAO climate map
Boreal and temperate forests		Sum of emissions from step 1 minus emissions from the humid tropical class above
Peat	Sum of emissions from all peatlands	
Savanna, grassland, and bushland fire	Sum of emissions from grassland, savanna, woody savanna, open shrubland, and closed shrubland (UMD classes 6–10)	

Emissions from all other land cover classes were grouped in the "savanna, grassland, and shrubland" class, consistently with the GFED4s emissions and were then analyzed against the latter. Peatland emissions were compared directly among the two datasets.

Comparison of emissions between GFED4s and FAOSTAT for all aggregated classes was performed in terms of CO_2eq emissions, obtained by summing up the CO_2, CH_4, and N_2O emissions for each source of emissions after conversion to CO_2eq by use of the Global Warming Potential (GWP) over 100 year time horizon (using the IPCC SAR values of $N_2O = 310$; $CH_4 = 21$).

GFED4s emissions are published in raster and tabular format, the latter aggregated by GFED regions (Giglio et al. 2013) and by source of emissions: savanna, grassland and shrubland, boreal forest, temperate forest, deforestation and forest degradation, peatland. The tabular values and the related regional distribution were employed for comparison with the new FAOSTAT emissions of this exercise. For ease of reference, GFED regions are illustrated in Fig. 1.

It should be noted that while the previous version of GFED emissions (GFED4) was directly calculated based on the C5.1 burned areas, the latest GFED4s dataset also include emissions from small fires (van der Werf et al. 2017).

3 Results

3.1 Comparison of burned areas

Giglio et al. (2018b) provides a comparison of C6 MCD64A1 and C5.1 MCD64A1 mean annual burned areas for the forest, shrubland, savanna, grassland, and cropland land cover classes, globally, and for the 14 sub-continental GFED regions and found that

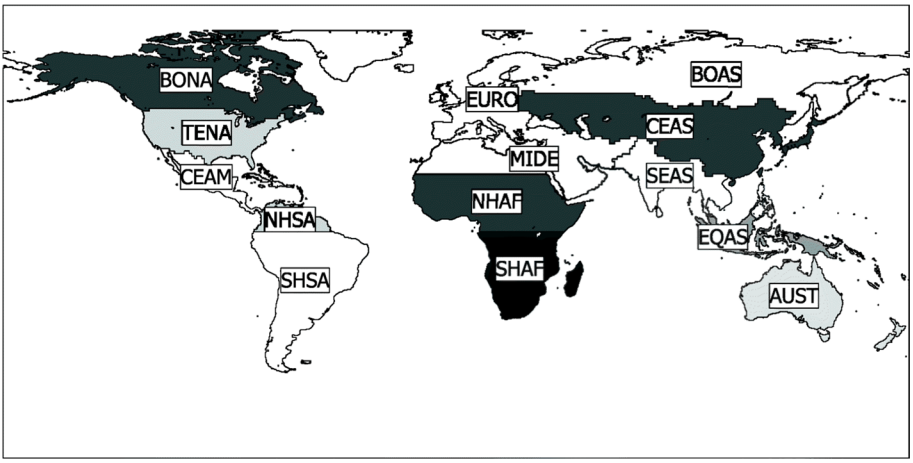

Fig. 1 GFED global regions for emissions as defined in Giglio et al. (2006). BONA Boreal North America; TENA Temperate North America; CEAM Central America; NHSA Northern Hemisphere South America; SHSA Southern Hemisphere South America; EURO Europe; MIDE Middle East; NHAF Northern Hemisphere Africa; SHAF Southern Hemisphere Africa; BOAS Boreal Asia; CEAS Central Asia; SEAS Southeast Asia; EQAS Equatorial Asia; AUST Australia and New Zealand

the new product detects significantly more burned area (26%) at global level and in almost every region, with the exception of boreal North America (BONA) where the mean annual area burned is 6% lower, possibly as a result of a large increase in the number of small lakes mapped at high latitudes (Giglio et al. 2018b). Differently from our exercise, however, Giglio et al. (2018b) used for 2014–2016 the 2013 MCD12Q1 land cover product and the C5.1 MCD12Q1 land cover product for previous years, as we did in FAOSTAT for the whole time series.

As mentioned in the data and methods section, in this study, we performed a similar comparison but partitioning the C6, C5.1, and GFED4s burned areas by the FAOSTAT land cover classes. We found that the average absolute difference in burned areas between C6 and C5.1 (C6 minus C5.1) over the full time series (i.e., the average difference between the respective sums of burned areas under all the land cover classes in all continents) is 61 M ha/year globally (− 29 Mha/year against GFED4s). On a yearly basis, the difference varies between 45 M ha and 72 M ha, with the C6 series always greater than C5.1, consistently with the results of Giglio et al. (2018b). The two series, however, show an almost perfect parallel trend, well reflected in the Pearson correlation coefficient ($\rho = 0.98$) (Fig. 2).

At the level of single-land cover class, the average yearly difference in burned areas (C6 minus C5.1) varies from 31 M ha for the savanna class (impacting for more than half of the total difference) to − 0.71 M ha for the peatland class, with quite substantial fluctuations on year to year basis (Fig. 3).

Other major differences in the total burned area can be observed in the land cover classes 7 (open shrubland, 14 M ha) and 8 (woody savanna, 11 M ha). These three classes account for more than 93% of the total difference, while forests are only responsible for a +7.2% increase in burned area (+2.3% the humid tropical forest, +4.9% the other forests) in C6 compared to C5.1.

The weakest relationship (i.e., the smallest Pearson coefficient) between the two data sets appears in class 10 (grassland) with $\rho = .562$. Finally, with the only exception of closed shrublands and grasslands, the annual burned area mapped globally by the C6 product is always greater than in the corresponding C5.1 product.

A more in-depth analysis on the geographical distribution of the burned areas differences reveals further details, as illustrated in Fig. 4, which also includes corresponding values from GFED4s partitioned as illustrated in Section 2.1. C6 consistently reports larger burned areas in peatlands than earlier version, mostly in boreal Asia (BOAS). Considering that fires in peatlands are calculated independently for any land cover, this appears due primarily to C6 increased capability to detect small burned areas.

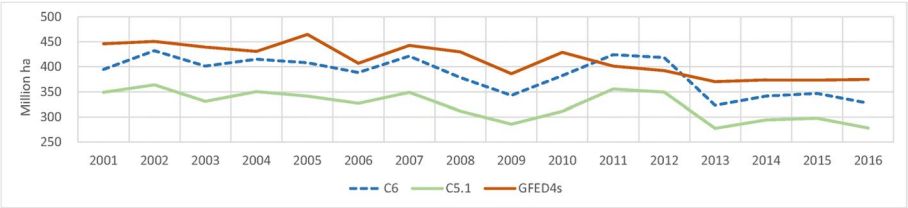

Fig. 2 Comparison of yearly global burned areas for the two indicated collections of MCD64A1 and GFED4s, considering all land cover types combined

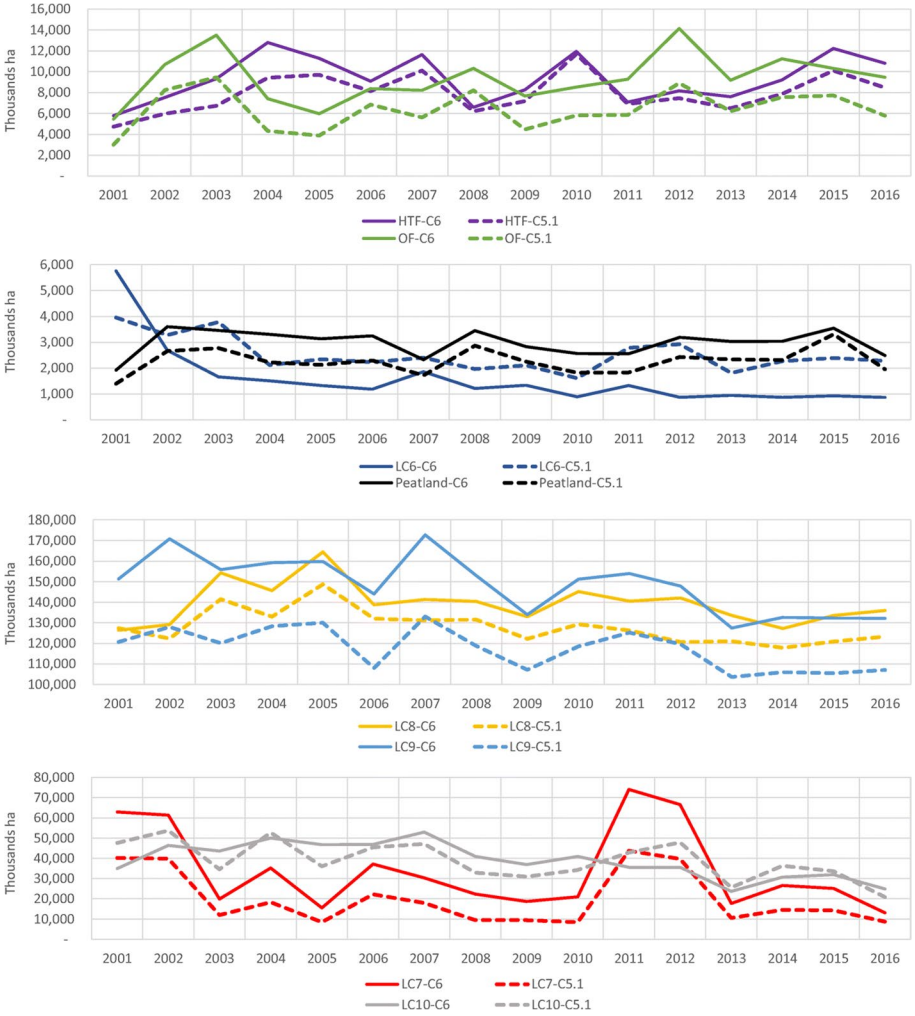

Fig. 3 Time series of trends for the MCD64A1 C6 and C5.1 burned area products at global level by land cover class (LC). LC6 closed shrubland, LC7 open shrubland, LC8 woody savanna, LC9 savanna, LC10 grassland, HTF humid tropical forest (deforestation and forest degradation), OF other forest (boreal and temperate). Values for the Pearson coefficient are LC6 = 0.704; LC7 = 0.991; LC8 = 0.868; LC9 = 0.953; LC10 = 0.562; HTF = 0.919; OF = 0.935; Peatland = 0.90

3.2 Emissions

Globally, the updated FAOSTAT emission estimates (i.e., considering all sources) are consistent with those of the GFED4s across the whole time series. FAOSTAT and GFED4s report mean global values of 7600 ± 359 Tg CO_2eq year^{-1} and 7115 ± 332 Tg CO_2eq year^{-1}, respectively (Pearson correlation coefficient of $\rho = 0.67$, statistically meaningful at $p < .05$, $\alpha = 0.49$), a difference of 484 ± 283 Tg CO_2eq year^{-1} or about 6%. Previous global FAOSTAT estimates using C5.1 were 6031 ± 254 Tg CO_2eq year^{-1} (Fig. 5).

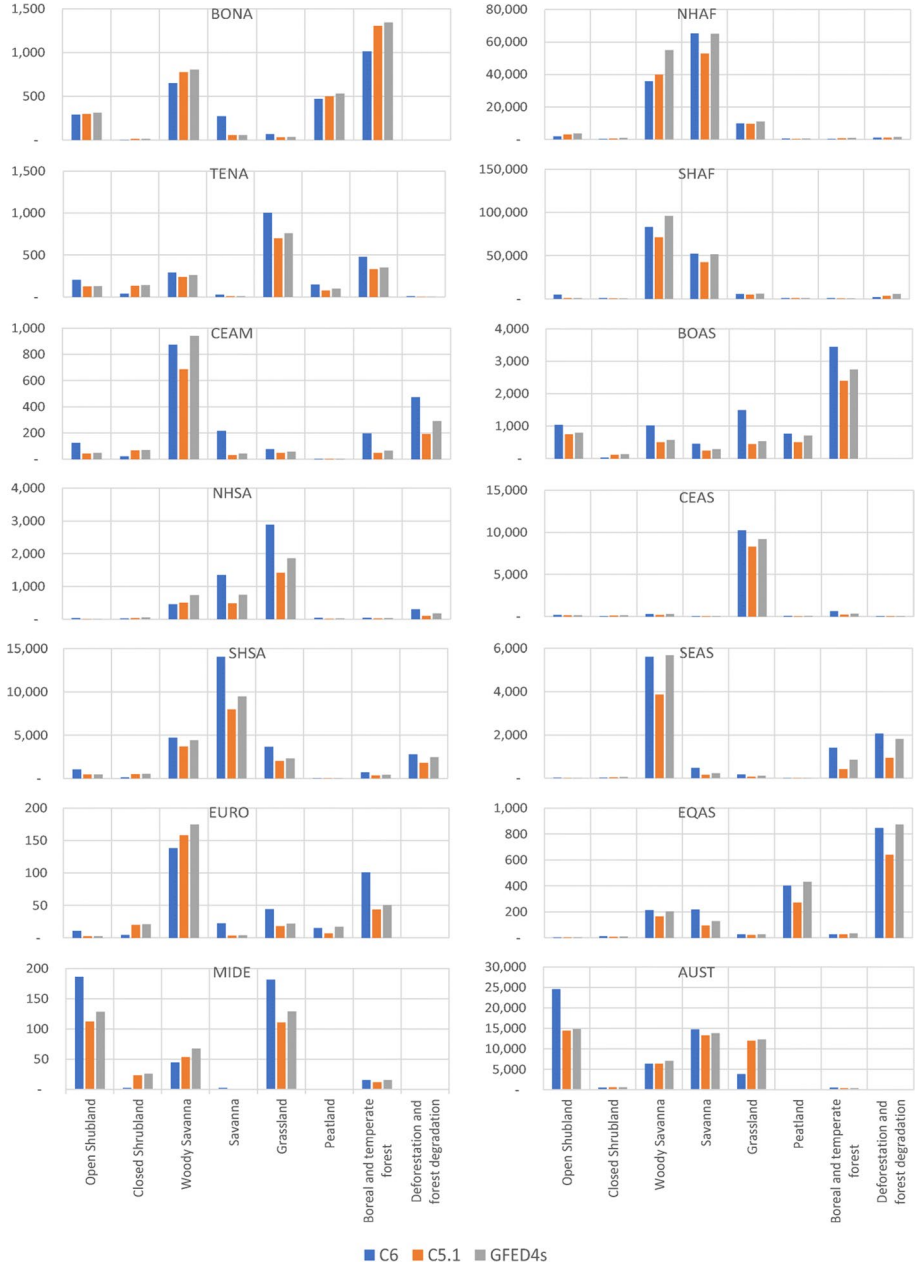

Fig. 4 Average annual burned areas by dataset, land cover class (plus peatland), and GFED region expressed as thousands of hectares for the years 2001–2016

In absolute terms, the class that most contributes to the noted difference between FAOSTAT and GFED4s at global level was peatland (i.e., FAOSTAT minus GFED4s was 1215 ± 161 Tg CO_2eq year^{-1}), followed by savanna, grassland, and shrubland combined classes (-556 ± 224

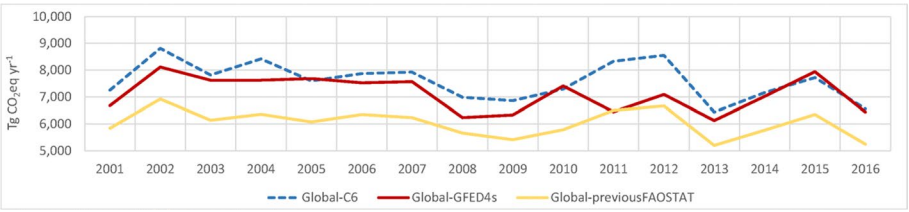

Fig. 5 Time trends of fire-related global CO_2eq emissions for all biomass types combined as resulting from GFED4s and the C6 exercise as well as the previous FAOSTAT. Statistical values are in Table 5

Tg CO_2eq year^{-1}), tropical deforestation (-209 ± 111 Tg CO_2eq year^{-1}) and finally the boreal and temperate forest class (35 ± 66 Tg CO_2eq year$^{-1)}$) (Table 3).

The analysis of global emissions at regional level indicates that the region contributing the most to the above differences is Australia and New Zealand (563 ± 200 Tg CO_2eq year^{-1}), followed by Southern Hemisphere South America (-348 ± 150 Tg CO_2eq year^{-1}), Northern Hemisphere Africa (200 ± 57 Tg CO_2eq year^{-1}), and temperate North America (126 ± 23 Tg CO_2eq year^{-1}). Other regions contribute for lesser amounts to the total differences (Fig. 6).

However, by looking at the single-source classes, the situation appears different. Table 4 illustrates a summary of the average annual emissions by source class and by region for the GFED4s and FAOSTAT datasets, complemented by figures from previous FAOSTAT (C5.1) estimates.

In the peatland class, FAOSTAT emissions are always higher than GFED4s in all regions and across the entire time series. Such pattern is more pronounced in the Southern Hemisphere Africa (accounting for 569 ± 34 Tg CO_2eq year^{-1}) and the Northern Hemisphere Africa (229 ± 33 Tg CO_2eq year^{-1}), and equally relevant in the temperate North America (109 ± 20 Tg CO_2eq year^{-1}) and boreal Asia (107 ± 25 Tg CO_2eq year^{-1}).

The reduced emissions in Southern Hemisphere Africa from savanna, grassland, and shrubland contribute with -598 ± 71 Tg CO_2eq year^{-1} to the overall difference in emissions with GFED4s, although they almost completely compensate the increased emissions in Australia and New Zealand (554 ± 199 Tg CO_2eq year^{-1}). The Southern Hemisphere South America increased emissions account for 210 ± 49 Tg CO_2eq year^{-1} in the differences with GFED4s, while Southeast Asia for -144 ± 21 Tg CO_2eq year^{-1}.

In the tropical forest class, Southern Hemisphere South America contributes -205 ± 107 Tg CO_2eq year^{-1} to the total difference, Equatorial Asia -125 ± 62 Tg CO_2eq year^{-1}, while other regions with smaller amounts.

For the boreal and temperate forest class, the noted differences are distributed so that a difference of -128 ± 44 Tg CO_2eq year^{-1} originates in the boreal North America region, -102 ± 57 Tg CO_2eq year^{-1} in the boreal Asia region whereas almost the same amount but with

Table 3 Absolute emissions for the given land cover classes and related standard error (in Tg CO_2eq year^{-1})

Dataset	Global	Peatland	Savanna, grassland, and shrubland	Deforestation and forest degradation	Boreal and temperate forests
C6	7600 ± 359	1459 ± 130	4455 ± 322	899 ± 106	787 ± 87
GFED4s	7115 ± 332	244 ± 123	5011 ± 185	1109 ± 196	752 ± 129
C5.1	6032 ± 254	1086 ± 100	3660 ± 240	768 ± 90	518 ± 70

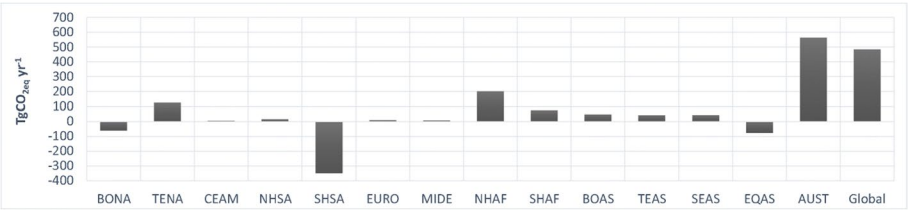

Fig. 6 Difference in average annual fire emissions for all biomass types combined calculated as C6 minus GFED4s by GFED region (in Tg CO_2eq year^{-1})

opposite sign (111 ± 27 Tg CO_2eq year^{-1}) is due to fires in Southeast Asia. Smaller differences in this class were computed in the remaining regions.

Notwithstanding the above region-specific differences in average yearly values, the Pearson correlations for the single-source classes at global level across the time series of the FAOSTAT and GFED4s datasets are all higher than the one of the combined sources and all statistically significant (at $p < .01$, $\alpha = 0.623$) as illustrated in Table 5. In the same table, t tests show a more mixed situation: the averages appear statistically similar for any sources (including all sources combined) except savanna and peatland, for which the value of p is also lower than the standard .05 level. The same test performed on current and previous FAOSTAT estimates confirms that the mean values by source class are always different (despite the high correlation) with the exception of the deforestation and forest degradation class.

4 Discussion and conclusions

4.1 Burned areas

The burned area comparison confirms other studies (Giglio et al. 2018b; Humber et al. 2019) highlighting that C6 burned areas differ substantially from those of C5.1 except for the grassland (UMD10) and the humid tropical forests classes. At the level of single GFED region, the situation is more mixed. However, there appears to be a high correlation in the two datasets as represented by the Pearson coefficient.

Collection 5.1 (and therefore previous FAOSTAT data) and the new C6 burned areas are based on two subsequent versions of the same algorithm applied to the same raw imagery as detected from the Aqua and Terra sensors combined. Significant differences in the amount of burned areas are observed due to changes and refinements operated on the underlying algorithm. From the product descriptions already, a first element can be drawn to confirm such statements. Indeed, compared to Collection 5.1, C6 product generally contains larger burned areas due to the presence of small fires and of an expanded coverage (i.e., a larger number of tiles are available). Previous studies (Tsela et al. 2014; Zhu et al. 2017; Mangeon et al. 2015) confirm that, with respect to ground truth data and/or other sources of information, Collection 5.1 underestimates the amount of surface burned especially where fire occurs on small and fragmented portion of lands, resulting in large omission errors.

Borini et al. (2018) confirmed the improvements of C6 compared to earlier MODIS products in the Brazilian Amazon, although other authors report more mixed results elsewhere. Fornacca et al. (2017) found that in a particular mountainous study area in

Table 4 Average annual emissions by source class and by GFED region for the GFED4s, FAOSTAT (C6), and previous FAOSTAT (C5.1) datasets (in Tg CO_2eq $year^{-1}$) along with some basic statistics

	Savanna, grassland, and shrubland			Deforestation and forest degradation			Boreal and temperate forest	
Dataset →→ Region ↓↓	GFED4s	FAOSTAT (C6)	FAOSTAT (C5.1)	GFED4s	FAOSTAT (C6)	FAOSTAT (C5.1)	GFED4s	FAOSTAT (C6)
BONA	0	13	13	0	0	0	204	75
TENA	17	17	16	0	1	0	26	43
CEAM	46	16	11	30	45	19	0	18
NHSA	74	48	25	21	29	10	0	4
SHSA	491	281	184	475	270	174	12	67
EURO	3	2	2	0	0	0	0	9
MIDE	0	6	5	0	0	0	0	1
NHAF	1373	1299	1232	68	92	90	0	21
SHAF	2270	1671	1317	135	183	322	0	57
BOAS	3	46	31	0	0	0	361	259
CEAS	62	79	66	1	0	0	36	52
SEAS	212	67	44	127	198	91	23	135
EQAS	51	5	3	205	80	62	0	3
AUST	349	904	710	6	1	1	32	44
GLOBAL	5011	4455	3660	1109	899	768	752	787
Statistics on "GLOBAL" figures								
STDEV	365	637	472	387	211	178	255	173
CV	0.073	0.143	0.129	0.349	0.235	0.232	0.339	0.219

	Boreal and temperate forest	Peatland			All classes combined		
Dataset →→ Region ↓↓	FAOSTAT (C5.1)	GFED4s	FAOSTAT (C6)	FAOSTAT (C5.1)	GFED4s	FAOSTAT (C6)	FAOSTAT (C5.1)
BONA	95	13	68	57	217	156	180
TENA	29	0	107	46	42	169	103
CEAM	4	0	2	1	76	82	35
NHSA	2	0	27	7	95	110	46

Table 4 (continued)

Dataset →→ Region ↓↓	Boreal and temperate forest	Peatland			All classes combined		
	FAOSTAT (C5.1)	GFED4s	FAOSTAT (C6)	FAOSTAT (C5.1)	GFED4s	FAOSTAT (C6)	FAOSTAT (C5.1)
SHSA	29	0	12	5	979	630	394
EURO	4	0	2	1	3	13	7
MIDE	1	0	0	0	0	8	6
NHAF	52	0	229	129	1440	1641	1536
SHAF	32	0	569	386	2404	2480	2156
BOAS	176	4	111	57	368	416	280
CEAS	20	0	10	4	100	142	91
SEAS	40	0	6	2	362	405	177
EQAS	3	217	292	166	474	396	278
AUST	30	0	1	1	388	951	742
GLOBAL	518	244	1459	1086	7115	7600	6032
Statistics on “GLOBAL” figures							
STDEV	138	243	258	195	656	709	502
CV	0.267	0.997	0.176	0.179	0.092	0.093	0.083

Table 5 *t* test and Pearson statistics of global fire emissions in the 2001–2016 interval, for GFED4s and new FAOSTAT estimates as well as for the new and previous FAOSTAT estimates (in Tg CO_2eq $year^{-1}$). The *t* test indicates that the averages of the two samples being tested are statistically similar when *t*-stat is comprised between ± *t* critical

		GFED4s—FAOSTAT C6			FAOSTAT C6—FAOSTAT C5.1		
	t test			Pearson	*t* test		Pearson
	t critical two tail	*t* stat	*p* Two tail	*ρ*	*t*-stat	*p* Two tail	*ρ*
Savanna, grassland, and shrubland	2.064	3.02	0.005	0.735	4	0	0.827
Deforestation and forest degradation	2.06	1.42	0.17	0.893	1.9	0.07	0.919
Boreal and temperate forest	2.07	1.9	0.07	0.881	4.85	0	0.923
Peatland	2.04	− 13.71	0	0.793	4.61	0	0.948
All sources combined	2.042	− 2	0.054	0.666	7.21	0	0.979

China, the detection performance of C6 on small fires (< 120 ha) was nevertheless lower than previous MODIS product MCD45A1, a result that was then confirmed by Giglio et al. (2018b). Similar conclusion was reported by Rodrigues et al. (2018) in the Brazilian Cerrado, by Zhu et al. (2017) in boreal Eurasia, and by Roteta et al. (2019) in sub-Saharan Africa.

For more detailed analysis on the differences among the burned areas, global and regional values as well as the science behind the different MODIS burned area products, including MCD64A1 C6 and C5.1, the reader is referred to Giglio et al. (2018b).

4.2 Emissions

Our analysis shows that the new FAOSTAT emission estimates from burning of biomass are, for most of the vegetation sources, highly correlated to those of GFED4s (i.e., the latest version of the Global Fire Emissions Database), despite the differences in burned area discussed in Section 4.1 above.

This is likely due to multiple and combined effects, which may include the following:

First of all, GFED4s emissions are calculated based on GFED4 burned areas plus the "boost" given by the burned areas from small fires. Therefore, GFED4s uses a set of burned areas that somewhat resembles the one of the C6 burned area product used herein. The increase in burned areas surface has the effect to also increase the overall emissions.

Secondly, GFED4s made several modifications from previous GFED versions in both input datasets and in the modeling framework (van der Werf et al. 2017), showing that the addition of small fires to the previous GFED4 had the largest impact on emissions in temperate North America, Central America, Europe, and Central Asia. Furthermore, the newly developed fuel biomass loads and fractions of biomass burnt appear, on average, to lower previous estimates of emissions (van der Werf et al. 2017). Thus, differences observed in Tables 3 and 4 may in part be due to these novel components. However, the new GFED4s elements such as revised methods for fuel consumption parameterization and representation of fuel consumption in frequently burning landscapes are more difficult to assess in isolation to quantify their role in observed discrepancies.

The observed variability of global GFED4s' and FAOSTAT mean emissions, measured with coefficients of variation, is similar (CV = 9.2% and CV = 9.3%, respectively) but generally higher for GFED4s data (except the savanna class) compared to FAOSTAT at the level of single sources. Rossi et al. (2016) explained such differences on the use of the dynamic CASA model by GFED to derive variable biomass combustion values as opposed to the static default IPCC values used in FAOSTAT.

In the peatland class, where both GFED and FAOSTAT employed fixed biomass combustion values, the difference in CV is maximum (CV = 99% compared to CV = 17%, respectively) likely due to the reduced coverage of the peatland map used in GFED (Table 4).

Indeed, more pronounced differences between FAOSTAT and GFED4s are observed in the peatland class, especially in the African and temperate Northern America but also in the Southern American regions. Indeed, an inverted trend between BONA and TENA emissions can be noted between C6 and GFED4s that depends mostly on peatland. However, this can be explained by the fact that in this class, C6 detects double the amount of burned areas in TENA, mostly in the portion of territory that falls within our tropical zone (where fuel biomass consumption is 353 t/ha compared to the temperate/boreal one 66 t/ha) and slightly lower an amount in BONA compared to C5.1 (Fig. 4). Therefore, the increased amount of tropical burned areas in TENA implies a more than proportional increase in emission for C6 compared to C5.1 and overall makes TENA emit more than BONA on average.

In other regions, even greater differences in peat fire emissions are observed, notably in Africa. Compared to peatlands in Equatorial Asia, peat and peat fires in Africa are poorly studied, although recent estimates (Dargie et al. 2017; Leifield & Menichetti 2018) indicate that the Congo basin is much richer in peat that presently known (Page et al. 2011, FAO/IIASA/ISRIC/ISSCAS/JRC 2012) and that climate change may induce extensive draught and higher risks of degradation. Palmer et al. (2019) reported unexpectedly large net emissions from tropical Africa in recent years especially from western Ethiopia and western tropical Africa, recalling the occurrence there of large soil organic carbon stores and the substantial land use change. Gumbricht et al. (2017) recognize that large biases hold in our current understanding of the distribution, area and volumes of tropical peat, and their continental contributions but propose that Southern America could be the region with richest peatlands endowment in the globe.

Our use of the map of histosols from the World Harmonized Soil database, which only captures part of these extensive peatlands in Africa and elsewhere, overlaid with the annual maps of burned areas as a proxy for burned peatlands suggests that relevant sources of emissions could reside in burned peatlands in these regions which were not highlighted in other global studies. As no ground verification is available at this time, more research is needed to assess the validity, plausibility, and likelihood of our possible findings. On the other hand, while earlier GFED versions traditionally limited the analysis of peat fires to tropical organic soils in Borneo and Sumatra (Giglio et al. 2010; Giglio et al. 2013) and GFED4s reports limited fire emissions from peatland in regions other than the Equatorial Asia, different definitions of peatland and of their geographical scope between FAOSTAT applications and GFED4s are likely responsible for the observed differences in peat fires, as discussed in Rossi et al. (2016).

In conclusion, our findings confirm the results of other studies (Giglio et al. 2018b; Humber et al. 2019) which show that the total area burned estimates vary greatly between products in terms of area burned and location. However, while this has significant implications for the use of global burned areas including for emissions applications, our results further support those of

Rossi et al. (2016), confirming that the FAOSTAT estimates using new burned area products are consistent with GFED4s at global and regional aggregation. Our analysis therefore confirms the comparability of tier 1–based emission estimates with those obtained applying a Tier 3 method based on the use of a far more complex mathematical model, and could represent a useful complementary tool in support of country GHG reporting to the UNFCCC.

Acknowledgments The authors wish to thank the reviewers for their careful refereeing and their insightful comments.

Funding information This research was carried out under the Mitigation of Climate Change in Agriculture (MICCA) program of the Food and Agriculture Organization of the United Nations (FAO), by the "Mitigation of GHG in Agriculture: Towards Wider Opportunities" (MAGHG2) project, financed by the German government (GCP/GLO/500/GER) and by the US National Aeronautics and Space Administration (NASA) grant number 80NSSC18K0400. The FAOSTAT database is developed and maintained by the FAO Statistics Division with FAO Regular Budget funding.

References

Borini Alves D, Pérez-Cabello F, Rodrigues Mimbrero M, Febrer-Martínez M (2018) Accuracy assessment of the latest generations of MODIS burned area products for mapping fire scars on a regional scale over Campos Amazônicos savanna enclave (Brazilian Amazon). J Appl Remote Sens 12(2):026026. https://doi.org/10.1117/1.JRS.12.026026

Boschetti L, Roy DP, Giglio L, Huang H, Zubkova M, Humber ML (2019) Global validation of the collection 6 MODIS burned area product. Remote Sens Environ 235:111490. https://doi.org/10.1016/j.rse.2019.111490

Ciais P, Sabine C, Bala G, Brovkin V, Canadell J, Chhabra A et al (2013) Carbon and other biogeochemical cycles. In: Stocker T, Qin D, Plattner GK et al (eds) Climate change 2013: the physical science basis. Contribution of working group I to the fifth assessment report of the intergovernmental panel on climate change. Cambridge University Press, Cambridge https://www.ipcc.ch/site/assets/uploads/2018/02/WG1AR5_Chapter06_FINAL.pdf.

Dargie GC, Lewis SL, Lawson IT, Mitchard ETA, Page SE, Bocko YE, Ifo SA (2017) Age, extent and carbon storage of the Central Congo Basin peatland complex. Nature 542:86–90. https://doi.org/10.1038/nature21048

EPA (2010) Methane and Nitrous Oxide Emissions From Natural Sources. United States Environmental Protection Agency. EPA 430-R 10-001 https://nepis.epa.gov/Exe/ZyPDF.cgi/P100717T.PDF?Dockey=P100717T.PDF Accessed November 2018

FAO/IIASA/ISRIC/ISSCAS/JRC (2012) Harmonized World Soil Database (version 1.2). FAO and IIASA

Fornacca D, Ren G, Xiao W (2017) Performance of three MODIS fire products (MCD45A1, MCD64A1, MCD14ML), and ESA Fire_CCI in a mountainous area of Northwest Yunnan, China, characterized by frequent small fires. Remote Sens 9:1131. https://doi.org/10.3390/rs9111131

Friedl MA, Sulla-Menashe D, Tan B, Schneider A, Ramankutty N, Sibley A, Huanga X (2010) MODIS collection 5 global land cover: algorithm refinements and characterization of new datasets. Remote Sens Environ 114:168–182. https://doi.org/10.1016/j.rse.2009.08.016

Giglio L, Loboda T, Roy PD, Quayle B, Justice CO (2009) An active-fire based burned area mapping algorithm for the MODIS sensor. Remote Sens Environ 113:408–420. https://doi.org/10.1016/j.rse.2008.10.006

Giglio L, Randerson JT, van der Werf GR, Kasibhatla PS, Collatz GJ, Morton DC, DeFries RS (2010) Assessing variability and long-term trends in burned area by merging multiple satellite fire products. Biogeosciences 7:1171–1186. https://doi.org/10.5194/bg-7-1171-2010

Giglio L, Randerson JT, van der Werf GR (2013) Analysis of daily, monthly, and annual burned area using the fourth generation global fire emissions database (GFED4). J Geophys Res-Biogeo 118:1–12. https://doi.org/10.1002/jgrg.20042

Giglio L, Boschetti L, Roy D, Hoffmann AA, Humber ML, Hall JV (2018a) Collection 6 MODIS Burned Area Product User's Guide. http://modis-fire.umd.edu/files/MODIS_C6_BA_User_Guide_1.2.pdf. Accessed October 2018

Giglio L, Boschetti L, Roy D, Humber ML, Justice CO (2018b) The Collection 6 MODIS burned area mapping algorithm and product. Remote Sens Environ 217:72–85. https://doi.org/10.1016/j.rse.2018.08.005

Gumbricht T, Roman-Cuesta RM, Verchot L, Herold M, Wittmann F, Householder E, Herold N, Murdiyarso D (2017) An expert system model for mapping tropical wetlands and peatlands reveals South America as the largest contributor. Glob Change Biol 23:3581–3599. https://doi.org/10.1111/gcb.13689

Hall JV, Loboda TV, Giglio L, McCarty GW (2016) A MODIS-based burned area assessment for Russian croplands: mapping requirements and challenges. Remote Sens Environ 184:506–521. https://doi.org/10.1016/j.rse.2016.07.022

Humber ML, Boschetti L, Giglio L, Justice CO (2019) Spatial and temporal intercomparison of four global burned area products. Int J Digit Earth 12(4):1–25. https://doi.org/10.1080/17538947.2018.1433727

IPCC (2006) In: Egglestone S, Buendia L, Miwa K, Ngara T, Tanabe K (eds) 2006 IPCC Guidelines for National Greenhouse Gas Inventories – Volume 4. Prepared by the National Greenhouse Gas Inventories Programme. Institute for Global Environmental Strategies, Japan

Levine JS (2010) Biomass burning. In: Reay D, Smith P, van Amstel A (eds) Methane and climate change. Earthscan, London, pp 97–114

Mangeon S, Field R, Fromm M, McHugh C, Voulgarakis A (2015) Satellite versus ground-based estimates of burned area: a comparison between MODIS based burned area and fire agency reports over North America in 2007. Anthropocene Rev 3(2):76–92. https://doi.org/10.1177/2053019615588790

Page SE, Rieley JO, Banks CJ (2011) Global and regional importance of the tropical peatland carbon pool. Glob Change Biol 17:798–818. https://doi.org/10.1111/j.1365-2486.2010.02279.x

Palmer PI, Feng L, Baker D, Chevallier F, Bösch H, Somkuti P (2019) Net carbon emissions from African biosphere dominate pan-tropical atmospheric CO2 signal. Nat Commun 10:3344. https://doi.org/10.1038/s41467-019-11097-w

Rossi S, Tubiello FN, Prosperi P, Salvatore M, Jacobs H, Biancalani R, House JI, Boschetti L (2016) FAOSTAT estimates of greenhouse gas emissions from biomass and peat fires. Clim Chang 135:699. https://doi.org/10.1007/s10584-015-1584-y

Roteta E, Bastarrika A, Padilla M, Storm T, Chuvieco E (2019) Development of a Sentinel-2 burned area algorithm: generation of a small fire database for sub-Saharan Africa. Remote Sens Environ 222:1–17. https://doi.org/10.1016/j.rse.2018.12.011

Shi Y, Matsunagaa T, Saito M, Yamaguchi Y, Chen X (2015) Comparison of global inventories of CO2 emissions from biomass burning during 2002–2011 derived from multiple satellite products. Environ Pollut 206:479–487. https://doi.org/10.1016/j.envpol.2015.08.009

Smith P, Bustamante M, Ahammad H, Clark H, Dong H, Elsiddig EA, Haberl H et al (2014) Agriculture, forestry and other land use (AFOLU). In: Edenhofer O, Pichs-Madruga R, Sokona Y, Farahani E, Kadner S, Seyboth K, Adler A et al (eds) Climate change 2014: mitigation of climate change, Contribution of Working Group III to the Fifth Assessment Report of the Intergovernmental Panel on Climate Change. Cambridge University Press, Cambridge

Tsela P, Wessels K, Botai J, Archibald S, Swanepoel D, Steenkamp K, Frost P (2014) Validation of the two standard MODIS satellite burned-area products and an empirically-derived merged product in South Africa. Remote Sens 6:1275–1293. https://doi.org/10.3390/rs6021275

Tubiello FN, Salvatore M, Rossi S, Ferrara AF, Fitton N, Smith P (2013) The FAOSTAT database of greenhouse gas emissions from agriculture. Environ Res Lett 8:015009. https://doi.org/10.1088/1748-9326/8/1/015009

Tubiello FN, Salvatore M, Cóndor Golec RD, Ferrara A, Rossi S, Biancalani R, Federici S, Jacobs H, Flammini A (2014) Agriculture, forestry and other land use emissions by sources and removals by sinks. FAO Statistics Division Working Paper Series ESS/14–02 http://www.fao.org/3/a-i3671e.pdf.

Tubiello FN (2019) Greenhouse gas emissions due to agriculture. In: Ferranti P, Berry EM, Anderson JR (eds) Encyclopedia of food security and sustainability, vol 1. Elsevier, pp 196–205. https://doi.org/10.1016/B978-0-08-100596-5.21996-3

van der Werf GR, Randerson JT, Giglio L, van Leeuwen TT, Chen Y, Rogers BM, Mu M, van Marle MJE, Morton DC, Collatz GJ, Yokelson RJ, Kasibhatla PS (2017) Global fire emissions estimates during 1997–2016. Earth Syst Sci Data 9:697–720. https://doi.org/10.5194/essd-9-697-2017

van Leeuwen TT, van der Werf GR, Hoffmann AA, Detmers RG et al (2014) Biomass burning fuel consumption rates: a field measurement database. Biogeosci Discuss 11:8115–8180. https://doi.org/10.5194/bgd-11-8115-2014

Zhu C, Kobayashi H, Kanayal Y, Saito M (2016) validation of MODIS MCD64A1 burned area in boreal Eurasia. Poster presented at the Japan Geoscience Union meeting 2016

Zhu C, Kobayashi H, Kanayal Y, Saito M (2017) Size-dependent validation of MODIS MCD64A1 burned area over six vegetation types in boreal Eurasia: large underestimation in croplands. Sci Rep 7:4181. https://doi.org/10.1038/s41598-017-03739-0

Affiliations

Paolo Prosperi[1] · Mario Bloise[1] · Francesco N. Tubiello[2] · Giulia Conchedda[2] · Simone Rossi[3] · Luigi Boschetti[4] · Mirella Salvatore[1] · Martial Bernoux[1]

[1] Climate and Environment Division, Food and Agriculture Organization of the United Nations, Rome, Italy

[2] Statistics Division, Food and Agriculture Organization of the United Nations, Rome, Italy

[3] Joint Research Centre, European Commission, Ispra, Italy

[4] Department of Natural Resources and Society, University of Idaho, Moscow, ID, USA